Cao, Yan; Yao, Hui; Wang, Zhijie; Kittisak Jermsittiparsert; Yousefi, Nasser

**Article**

# Optimal Designing and Synthesis of a Hybrid PV/Fuel cell/ Wind System using Meta-heuristics

Energy Reports

**Provided in Cooperation with:**
Elsevier

*Suggested Citation:* Cao, Yan; Yao, Hui; Wang, Zhijie; Kittisak Jermsittiparsert; Yousefi, Nasser (2020) : Optimal Designing and Synthesis of a Hybrid PV/Fuel cell/Wind System using Meta-heuristics, Energy Reports, ISSN 2352-4847, Elsevier, Amsterdam, Vol. 6, pp. 1353-1362, https://doi.org/10.1016/j.egyr.2020.05.017

This Version is available at:
https://hdl.handle.net/10419/244133

Energy Reports 6 (2020) 1353–1362

Contents lists available at ScienceDirect

Energy Reports

journal homepage: www.elsevier.com/locate/egyr

Research Paper

# Optimal Designing and Synthesis of a Hybrid PV/Fuel cell/Wind System using Meta-heuristics

Yan Cao [a], Hui Yao [a], Zhijie Wang [a], Kittisak Jermsittiparsert [b,*], Nasser Yousefi [c]

[a] School of Mechatronic Engineering and Shaanxi Key Laboratory of Non-Traditional Machining, Xi'an Technological University, Xi'an 710021 China
[b] Social Research Institute, Chulalongkorn University, Bangkok 10330, Thailand
[c] Islamic Azad University, Karaj Branch, Iran

ARTICLE INFO

*Article history:*
Received 29 January 2020
Received in revised form 4 April 2020
Accepted 19 May 2020
Available online xxxx

*Keywords:*
Hybrid system
Lithium-ion battery
Proton exchange membrane fuel cell
PV
Wind
Elephant herding optimization algorithm
Lévy flight

ABSTRACT

In this paper, a multi-objective optimization method has been established on a hybrid PV, wind, fuel cell, and battery system. The optimization is based on three models including energy supply reliability, electricity efficiency, and capital cost of the hybrid system. A new model of the Elephant Herding Optimization (BEHO) Algorithm is utilized to solve the multi-objective optimization problem and is validated based on different algorithms and benchmark functions. The main purpose is to determine the Pareto surface including a set of possible design solutions to help the decision-makers obtaining the global optimum solution. The final results indicated that the proposed method is an applicable approach for designing of the proposed hybrid system.



## 1. Introduction

The world's orientation toward energy and moving toward an oil-free economy on the one hand and the various advantages of renewable energies, on the other hand, make it imperative to prioritize the development of these clean energies with various economic and environmental benefits (Liu et al., 2020). Improving citizens' awareness of the benefits of using renewable energies will certainly facilitate the development of cleaner energy in the world (Fathi et al., 2020). Special capacity for economic development, promotion of energy supply and security and environmental protection and reduction of air pollution are three important advantages of renewable energies. Also, the need to diversify the country's energy basket to improve energy security is another reason for the need to develop renewable energies. This is one of the priorities of the energy sector in light of the dramatic increase in energy demand in the coming years (Kiran and Chandrakala, 2020).

The scarcity of power grids in remote areas and the high cost of connecting these areas to national electricity networks lead to the use of other energy sources independently of the grid. One of the major problems with the use of renewable sources is the severity of the winds during the day and the lack of solar energy at night, which combines wind and solar systems (Fathi et al., 2020; Aghajani and Ghadimi, 2018). These hybrid systems also have some problems such as low system reliability and lack of peak load during the year. To resolve this problem, different solutions can be proposed (Liu et al., 2017; Gollou and Ghadimi, 2017). One of the useful, new, and widely used method is to adopt fuel cells as the storage system of these systems. Several works have been performed in this orientation. For example, Mirzapour et al. (2019) presented and optimized a hybrid system based on fuel cell, biomass gasifier generator set, power conditioning unit, and battery backup for an academic section in Maulana Azad National Institute of Technology in India. The HOMER simulator was adopted for designing the grid and it simulated the financial criteria of the system (Hosseini Firouz and Ghadimi, 2016; Hamian et al., 2018; Leng et al., 2018; Akbary et al., 2019; Ebrahimian et al., 2018). The examination was executed in different conditions. The simulation results showed that the cost of energy (COE) for the biomass gasifier generator set, solar PV, and fuel cell crossover energy system has is about15 Rs/kWh and complete net present cost (NPC) is 52 Rs/kWh.

Khodaei et al. (2018) proposed an optimized techno-economic grid-connected hybrid system including wind, solar, and fuel cell for residential applications. The storage system was utilized for increased system reliability. Different parameters of the system were analyzed to achieve their effectiveness on the system, The Genetic Algorithm (GA) and the Particle Swarm Optimization algorithm were utilized for minimizing the system maintenance and operation cost. Final results showed the

* Corresponding author.
*E-mail address:* kittisak.j@chula.ac.th (K. Jermsittiparsert).

https://doi.org/10.1016/j.egyr.2020.05.017

**Nomenclature**

| | |
|---|---|
| $A_s$ | Area of a single PV cell ($m^2$) |
| $C_T$ | Tafel constant |
| $E$ | Nernst Potential ($\upsilon$) |
| $f_{maintenence}$ | Maintenance factor of SOFC |
| F | Faraday constant |
| $i_{capital}$ | Capitalization ratio |
| I | Fuel cell stack current ($A$) |
| J | Current densities |
| N | Number of tubes |
| $N_b$ | Lifespan of batteries (year) |
| $N_p$ | Lifespan of project (year) |
| $N_{units}$ | Production volume of SOFC |
| N | Number of cells |
| P | Pressure |
| $R$ | Resistance ($\Omega$) |
| $R_c$ | Connections resistance |
| $R_m$ | Membrane resistance |
| S | Membrane area ($cm^2$) |
| $S_s$ | Salvage value of PV panels ($/$m^2$) |
| T | Temperature (°C) |
| U | Hydrogen utilization factor |
| V | Voltage ($\upsilon$) |

**Greek letters**

| | |
|---|---|
| $\alpha$ | Thermal voltage timing completion factor ($V$) |
| $\alpha_b$ | Initial cost of batteries ($/$m^2$) |
| $\alpha_s$ | Initial cost of PV panels ($/$m^2$) |
| $\alpha_{OMs}$ | Yearly operation and maintenance cost for solar ($/$m^2$ year) |
| $\beta$ | Parametric coefficient |
| $\lambda$ | Tunable parameter |
| $\gamma$ | Interest rate |
| $\kappa$ | Inflation rate |
| $\nu$ | Escalation rate |
| $\eta$ | Efficiency |
| $\xi$ | Pseudo-experimental parametric coefficients |
| $\Omega$ | Ohmic loss |
| $\tau$ | Solar radiation ($W/m^2$) |

**Subscripts**

| | |
|---|---|
| a | Activation |
| b | Battery |
| C | Capacitance |
| c | Concentration |
| $CO_2$ | Oxygen concentration at the cathode/gas interface (mol $cm^{-3}$) |
| $CH_2$ | Hydrogen concentration at the anode membrane /gas interface (mol $cm^{-3}$) |
| elec | Electrolyzer |
| FC | Fuel cell |
| G | Electrical energy that is generated by the PV |

method's prominence characteristics in using as cooling, heating, and
power source (CHP).

Bagal et al. (2018) studied a hybrid PV-Wind-Fuel Cell system and then, they optimized it for electricity production for remote sites in the Colombian Caribbean region. For performance analysis of the studied system, its simulation was applied to the demand of 200 W by considering the wind speed and the solar radiation variations for every single day in different regions. A multi-objective optimization was implemented to the study for minimizing the Levelized CO2 emission and energy cost.

Gheydi et al. (2016) proposed a three-part hybrid system based on the thermal solar system, wind turbine and, and fuel cell. The presented system allowed to maximize the yearly generated electricity based on the supplied power optimizing yearly. The method was then applied to a practical case study in Lebanon. The final results showed a secure achievement toward different renewable energy sources variations.

Firouz and Ghadimi (2016) proposed an adaptive multi-agent management system for a CHP system in micro-grid. The CHP system contained three parts: wind turbine, Fuel cell, and PV. The controller for the system was based on a fuzzy controller. The main objective was to design the load frequency controller (LFC) to control the frequency oscillation of the agents and to minimize the production cost of the overall system. The PSO algorithm was used to the optimal selection of the key parameters of the controller to adjust the system efficiency.

Eslami et al. (2019) investigated a combine CHP system including PV, wind, fuel cell, and battery for a nursing home in Istanbul. The study used HOMER software to characterize the optimal configuration of the hybrid system by considering the cost of energy and the total NPC. Simulation results showed the best configuration for the hybrid system.

Based on the literature, there is a lot of researches that worked on the optimal unit sizing of the hybrid solar-wind DG system. This study presents a new configuration by combining a high-temperature polymer electrolyte membrane fuel cell (PEMFC) system (including the electrolyzer and the fuel cell stacks) with the hybrid wind/PV system. The system presents a multi-objective optimization technique by considering the efficiency, energy reliability, and cost of the hybrid model.

## 2. Mathematical modeling of the overall system

The analyzed model in this study is a hybrid model including wind turbine, fuel cell, and solar system with electrolyzer and cell stacks (wind/solar/fuel cell) to use during a long time with storing the energy for the required times. In the operation process, the surplus electrical energy which is produced by PV and wind is adopted for producing hydrogen using electrolyzer. Afterward, the generated hydrogen is stored in hydrogen reservoir tanks. The hydrogen reservoir tanks are then employed to generate electricity by supplying fuel cell stacks. Fig. 1 indicates an energy management technique for the proposed hybrid DG based on (Saeedi et al., 2019).

### 2.1. Model of the fuel cell stack

This research utilizes a proton exchange membrane fuel cell (PEMFC) in the system due to its several advantages such as its higher efficiency and simple working. The model of the PEMFC stack is based on a steady-state model. The water is assumed as the membrane electrolyte saturator that makes it be a function of temperature. Fig. 2 shows a simple circuit model of a PEMFC.

Thereupon, the PEMFC current density depends on the geometric features, the reactants quantity, and the hydrogen utilization factor.

$$I_{FC} = \frac{2 \times n_{H_2,in} \times U_{FC}}{N_{FC} \times A_{FC}} \quad (1)$$

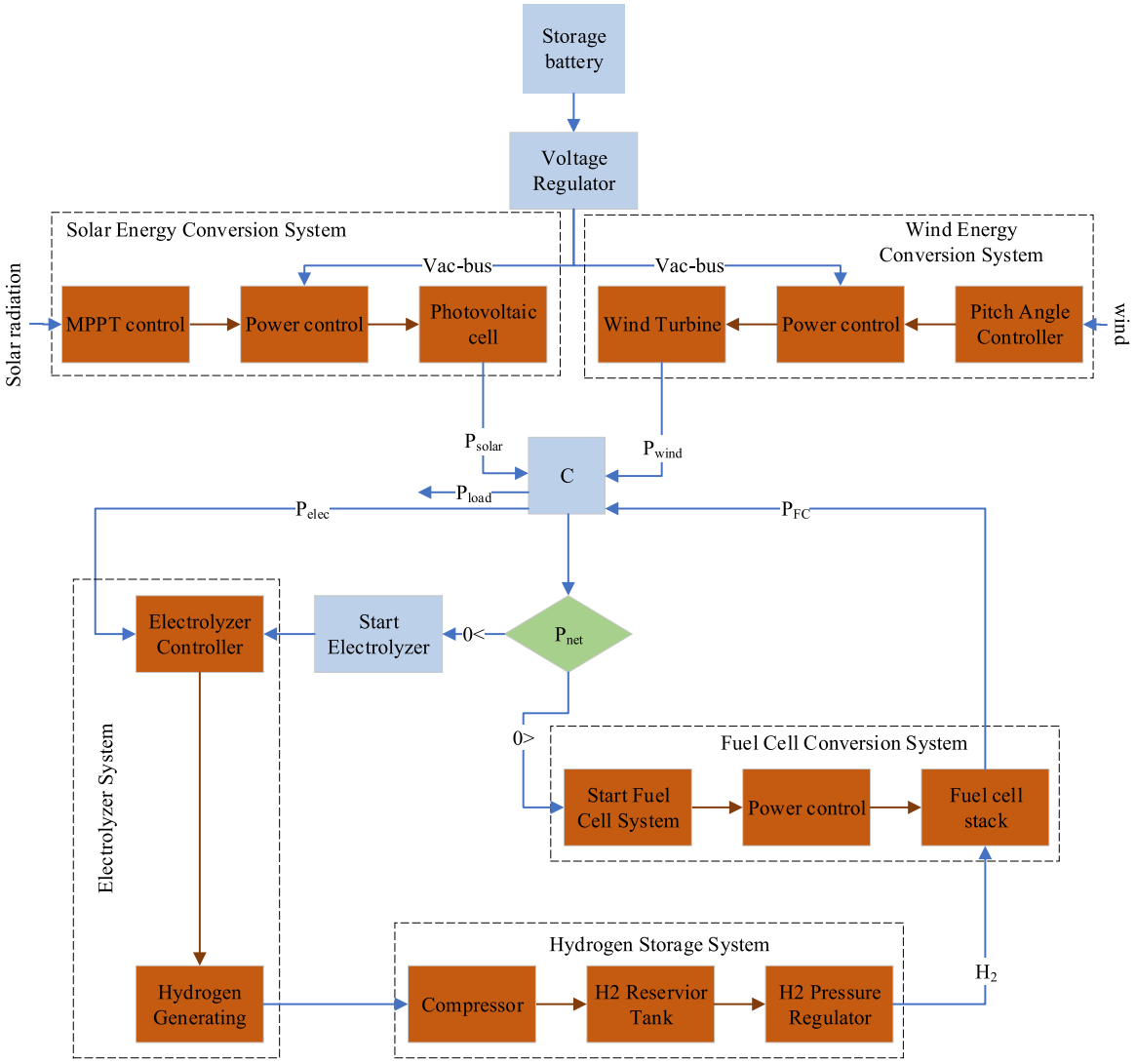


**Fig. 1.** The graphical conception of the energy management system for the presented hybrid system.

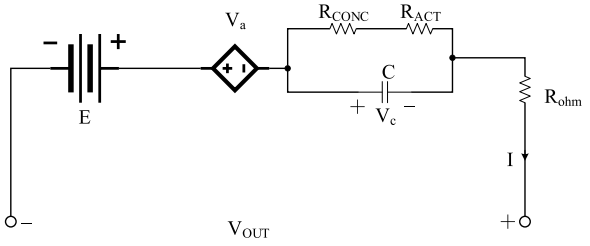


**Fig. 2.** The circuit model of a PEMFC.

where, $n_{H_2,in}$ stands for the number of $H_2$ tubes, $U_{FC}$ describes the hydrogen utilization factor, $N_{FC}$ is the cells number, and $A_{FC}$ is the active area.

Following Fig. 2, the PEMFC output voltage is achieved can be achieved based on the following equation:

$$V_{OUT} = E - V_a - V_C - V_\Omega \tag{2}$$

where, $V_a$ describes the activation loss voltage, $V_C$ determines the concentration losses voltage, $V_\Omega$ stands for the ohmic losses voltage, and $E$ describes the Nernst (reversible) potential and is achieved as follows:

$$E = 1.23 + \left(-8.5 \times 10^{-4}\right) \times (T_{FC} - 298.15) + \frac{RT_{FC}}{4F} ln\left(P_{H_2}\sqrt{P_{O_2}}\right) \tag{3}$$

The activation loss decreases the reactions speed on the electrode's surface and can be formulated by the following equation:

$$V_a = -0.95 + \times T + 7.6 \times 10^{-5} \times T \times ln\,(CO_2) + 1.93 \times 10^{-4} \times T \times ln\,(I_{FC}) \tag{4}$$

where, $I_{FC}$ describes the PEM fuel cell stack current and $CO_2$ determines the oxygen concentration at the cathode/gas interface (mol $cm^{-3}$) by the following:

$$CO_2 = \frac{p_{O_2} \times e^{\left(\frac{498}{T}\right)}}{50.8 \times 10^7} \tag{5}$$

where, $P_{O_2}$ stands for oxygen partial pressures ($Pa$).

And $\xi$ describes the pseudo-empirical parametric and this (Restrepo et al., 2014).

$$\xi = 0.003 + 0.0002 ln\,(A) + 43 \times 10^{-6} ln\left(C_{H_2}\right) \tag{6}$$

And $CH_2$ stands for the Hydrogen concentration at the anode membrane/gas interface (mol $cm^{-3}$) and is achieved as follows:

$$CH_2 = \frac{p_{H_2} \times e^{\left(\frac{-77}{T}\right)}}{10.9 \times 10^7} \tag{7}$$

where, $pH_2$ describe the hydrogen partial pressures ($Pa$).

The Ohmic voltage drop for the fuel cells is modeled by the following:

$$V_\Omega = I_{PEM}(R_m + R_c) \tag{8}$$

where,

$$R_m = \rho_m l S^{-1} \tag{9}$$

$$\rho_m = \frac{181.6 \times \left[0.062\left(\frac{T_{FC}}{303}\right)^2\left(\frac{I_{FC}}{S}\right)^{2.5} + 0.03\left(\frac{I_{FC}}{S}\right) + 1\right]}{\left[\lambda - 0.063 - 3\left(\frac{I_{FC}}{S}\right)\right] \times e^{\frac{T_{FC}-30}{T_{FC}}}} \tag{10}$$

where, $S$ stands for the membrane area ($cm^2$), $I$ describes the membrane thickness, $I_{FC}$ determines the PEMFC operating current, $T_{FC}$ represents the operating cell temperature ($K$), $\lambda$ determines a tunable parameter, $R_c$ and $R_m$ describe the connections resistance and membrane resistance, and $\rho_m$ stands for the resistivity of the membrane.

Finally, the concentration overvoltage can be also obtained based on the following equations:

$$V_C = -\beta \times ln\left(J_{max} - \frac{J}{J_{max}}\right) \tag{11}$$

where, $\beta$ stands for the parametric coefficient, $J$ and $J_{max}$ describes the typical and the maximum current densities, respectively.

### 2.2. Model of electrolyzer

The model of the electrolyzer is performed by the following assumption:

In the electrolyzer model, the water vapor of the electrolytic cells in the anode and the cathode are fully saturated and incompressible. The value of the temperature and the pressure for the electrolytic cells in gas flow channels are considered constants. The liquid and the gas phases are assumed separable. The enthalpy of the water vapor has been assumed constant during the working temperature. The working temperature for the electrolytic cells is considered 100 °C. The required energy for water supply and hydrogen compressing has been neglected.

The system cannot receive the maximum value that is due to the parasitic current losses. By considering the Faraday Law, the experimental hydrogen rate is achieved by the following equation (Guo et al., 2017):

$$\eta_I = 96.5 \times e^{\left(\frac{0.09}{I_{el}} - \frac{75.5}{I_{el}^2}\right)} \tag{12}$$

where, $\eta_I$ describes the current efficiency and $I_{el}$ represents the electrolyzer current density ($A/cm^2$).

And the rate of hydrogen production (mol/s) is obtained as follows:

$$r_{hp} = \frac{\eta_I \times I_{el} \times N_{el}}{2 \times F} \tag{13}$$

where, $N_{el}$ describes the number of electrolytic cells, $I_{el}$ stands for the electrolyzer current ($A$), $F$ determines the Faraday constant ($F = 96487$ C/mol).

Based on the explained assumptions, the Nernst equation ($E$) is considered to evaluate the reversible potential of the electrolytic cells that are explained before. The electrolytic cells have some unavoidable losses like ohmic, concentration polarization, and activation losses, the open-circuit voltage is greater than E. By neglecting the concentration overpotential loss due to its small value in electrolyzer cells (Yang et al., 2007), the open-circuit voltage can be formulated as follows:

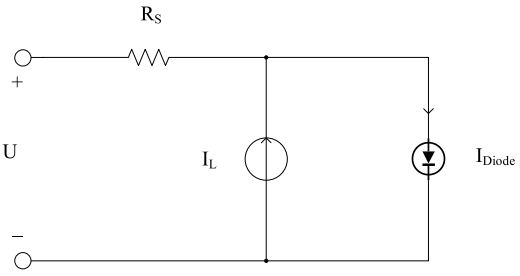


**Fig. 3.** The circuit model of a PV cell/module model.

$$V_{el} = E + V_{el}^{\Omega} + V_{el}^{a} \tag{14}$$

where, $V_{el}^{\Omega}$ describes the ohmic polarization loss for the cells ($V$), and $V_{el}^{a}$ represents the activation polarization loss for the electrolytic cells ($V$) and is obtained by the following equation (Hoogers, 2002):

$$V_{el}^{a} = C_T + S_T lgi \tag{15}$$

where, $C_T = 0.06$ describes the Tafel constant, and $S_T = 0.1$ represents the Tafel slope.

Finally, the Ohmic Voltage loss is obtained as follows:

$$V_{el}^{\Omega} = 0.127 \times I_{el} \times e^{-2870 \times \left(\frac{1}{1273} - \frac{1}{T_{el}}\right)} \tag{16}$$

### 2.3. Model of PV cell/module

A simple circuit-based model of a PV cell can be determined by four parameters that are shown in Fig. 3. Based on Fig. 3, the load current can be achieved as follows (Chen et al., 2017).

$$I = I_L - I_D = I_L - I_o \times \left[\exp\left(U + \frac{I \times R_s}{\alpha} - 1\right)\right] \tag{17}$$

where $U$ stands for the output voltage, $I_o$ represents the saturation current ($A$), $R_s$ describes the series resistance ($r$), $\alpha$ describes the thermal voltage timing completion factor ($V$), and $I_L$ describes the light current ($A$) and is achieved by the following equation.

$$I_L = \frac{\mathfrak{r}}{\mathfrak{r}_{ref}} \times \left[I_L^{ref} - Ct_I^{ref} \times \left(T_c - T_c^{ref}\right)\right] \tag{18}$$

where $\mathfrak{r}$ stands for solar radiation ($W/m^2$), $\mathfrak{r}_{ref}$ is the reference solar radiation that is assumed 1000 ($W/cm^2$), $I_L^{ref}$ describes the light currently at reference condition, $Ct_I^{ref}$ represents the temperature coefficient of the short-circuit current that is considered $A/25$ °C, and $T_c$ and $T_c^{ref}$ are the temperature of a PV cell (°C) and the reference temperature with value 25 °C, respectively.

The PV efficiency is highly affected by the temperature and the temperature is highly affected by different parameters such as solar radiation, output voltage, output current, and the ambient temperature. The relation between the PV module and the temperature is given in the following:

$$C_{PV} \times \frac{dT_c}{dt} = ra_{PV} \times \mathfrak{r} - \frac{U \times I}{A_r} - C_{ht}\left(T_c - T_a\right) \tag{19}$$

where, $C_{PV}$ represents the total heat capacity per unit area of the solar cell/module )J/(°C $m^2$)], $ra_{PV}$ describes the absorption rate for PV cells radiation, $C_{ht}$ stands for the heat transfer coefficient [W/(°C $m^2$)]. $T_a$ stands for the ambient temperature (°C). $A_r$ describes the PV cell absorption area ($m^2$)

### 2.4. Model of wind energy conversion system

The generator of the wind turbine model is achieved based on the following formula (Chedid et al., 1998):

$$P_{WTG} = \begin{cases} 0 & v < v_{ci} \\ \dfrac{P_r \times \left(v^3 - v_{ci}^3\right)}{v_r^3 - v_{ci}^3} & v_{ci} \le v \le v_r \\ P_r & v_r \le v \le v_{co} \\ 0 & v > v\_co \end{cases} \tag{20}$$

where, $v_{ci}$ stands for the cut-in wind speed, $v$ represents the local wind speed, $v_{co}$ describes the cut-out wind speed, and $v_r$ defines the rated wind speed for the wind turbine generator. Besides, the output power for the wind turbine is obtained by the following equation:

$$P_W = P_{WTG} \times A_W \times \eta_w \tag{21}$$

where, $\eta_w$defines the wind turbine generator efficiency where according to Betz's law, is no more than 16/27 (59.3%) of the kinetic energy in wind and $A_W$ stands for the swept area of it ($m^2$).

### 2.5. Model of battery

In this part, a simple model of lead–acid has been employed. The model is considered by identical charge and discharge efficiencies about 0.88. To prevent the deep discharge, 20% capacity of the batteries does not take part in the charging/discharging processes. The left-over electricity of the battery when it is charged can be obtained as follows:

$$\begin{cases} P_{re} = P_{re} + 0.88 \times P_i^{ch} & P_i^{ch} \times 0.88 \ge P_C \\ P_{re} = P_C & P_i^{ch} \times 0.88 \le P_C \end{cases} \tag{22}$$

And the left-over electricity of the battery when it is discharged is achieved as follows:

$$\begin{cases} P_{re} = P_{re} - 0.88 \times P_i^{ch} & \dfrac{P_{re} - P_i^{dis}}{0.88} \ge 0.20 \times P_C \\ P_{re} = P_C & \dfrac{P_{re} - P_i^{dis}}{0.88} \le 0.20 \times P_C \end{cases} \tag{23}$$

where, $P_{re}$ stands for the left-over electricity of the lead–acid battery, $P_C$ describes the battery capacitance, $P_i^{ch}$ and $P_i^{dis}$ represent the electric energy charging/discharging into/from the battery.

## 3. Objective function for the cost

The total cost of the proposed hybrid PV/wind/PEMFC/battery is defined by an objective function as follows:

$$C_T = C_{PV} + C_{wind} + C_{PEMFC} + C_{battery} \tag{24}$$

Such that the cost of the PV conversion system, the storage battery, and a wind energy conversion system is obtained by the following:

### 3.1. The cost model of the PV conversion system

The total cost of photovoltaic conversion system is achieved as follows:

$$C_{PV} = \frac{I_{PVs} - S_{PVs} + Cm_{PVs}}{N_p} \tag{25}$$

where, $N_p$ describes the lifespan of the project, $I_{PV}$ describes the initial cost of the PV energy conversion system as follows:

$$I_{PV} = \alpha_s \times A_s \tag{26}$$

The $S_{PVs}$ is the PV energy conversion system salvage value and is obtained as follows:

$$S_{PVs} = S_s \times A_s \times \left(\frac{1+\kappa}{1+\gamma}\right)^{N_p} \tag{27}$$

The $Cm_{PVs}$ determines the maintenance cost of PV energy conversion system and is achieved as follows:

$$Cm_{PVs} = \alpha_{cm_{PVs}} \times A_s \times \sum_{i=1}^{N_p} \left(\frac{1+\nu}{1+\gamma}\right)^i \tag{28}$$

### 3.2. The cost model of the wind conversion system

The total cost of the wind energy conversion system is achieved by the following formulation:

$$C_{wind} = \frac{I_{wind} - S_{wind} + Cm_{wind}}{N_p} \tag{29}$$

where, $N_p$ describes the lifespan of the project, $I_{wind}$ describes the initial cost of the wind turbine generator as follows:

$$I_{PV} = \alpha_{wind} \times A_{wind} \tag{30}$$

The $S_{wind}$ is the wind turbine generator system salvage value and is obtained as follows:

$$S_{wind} = S_{wind} \times A_{wind} \times \left(\frac{1+\kappa}{1+\gamma}\right)^{N_p} \tag{31}$$

The $Cm_{wind}$ determines the maintenance cost of the wind turbine generator system and is obtained by the following formulation:

$$Cm_{wind} = \alpha_{cm_{wind}} \times A_{wind} \times \sum_{i=1}^{N_p} \left(\frac{1+\nu}{1+\gamma}\right)^i \tag{32}$$

### 3.3. The cost model of the battery

The total cost of the battery is considered as follows:

$$C_{battery} = \frac{I_{battery} + Cm_{battery}}{N_p} \tag{33}$$

where, $I_{battery}$ stands for the initial cost of the lead–acid battery and is achieved as follows:

$$I_{battery} = \alpha_{battery} \times P_C \times \sum_{i=1}^{N_b} \left(\frac{1+\nu}{1+\gamma}\right)^{\frac{i-1}{N_b}} \tag{34}$$

The $Cm_{battery}$ determines the maintenance cost of the lead–acid battery and is obtained as follows:

$$Cm_{battery} = \alpha_{cm_{battery}} \times P_C \times \sum_{i=1}^{N_p} \left(\frac{1+\nu}{1+\gamma}\right)^i \tag{35}$$

### 3.4. The cost model for the PEMFC

The capital cost of the PEM fuel cell based on (Tan et al., 2015) is as follows:

$$C_{PEMFC} = \left(C_{PEMFC}^{purchase} + C_{PEMFC}^{maintenence} + C_{PEMFC}^{amortization}\right) \times \left(\frac{N_{units}}{500000}\right)^{-0.362} \tag{36}$$

where,

$$C_{PEMFC}^{purchase} = 1.1 \times [0.027 \times A_{PEMFC} + 0.88] \times N_{PEMFC} + 0.24 \times N_{PEMFC} + 279.4 \tag{37}$$

**Table 1**
The details for parameters utilized in the hybrid system model.

| Parameter | Value | Unit | Parameter | Value | Unit |
|---|---|---|---|---|---|
| $N_p$ | 20 | year | $\nu$ | 12 | % |
| $N_b$ | 10 | year | $A_{PEMFC}$ | 1.5 | $m^2$ |
| $\alpha_s$ | 450 | $/$m^2$ | $S_s$ | 45 | $/$m^2$ |
| $\alpha_{cm_{PVs}}$ | 4.3 | $/$m^2$ year | $\gamma$ | 12 | % |
| $\alpha_{cm_{wind}}$ | 2.5 | $/$m^2$ year | $N_{units}$ | 1482 | – |
| $\alpha_{battery}$ | 100 | $/$m^2$ | $f_{maintenence}$ | 0.06 | – |
| $\alpha_{wind}$ | 100 | $/$m^2$ | $i_{capital}$ | 10 | % |
| $\alpha_{cm_{battery}}$ | 10 | $/$m^2$ year | $S_{wind}$ | 10 | $/$m^2$ |
| $\kappa$ | 9 | % | | | |

$$C_{PEMFC}^{maintenence} = f_{maintenence} \times C_{PEMFC}^{purchase} \tag{38}$$

$$C_{PEMFC}^{amortization} = i_{capital} \times C_{PEMFC}^{purchase} \tag{39}$$

where, $N_{units}$ represents the production volume of the PEMFC, $f_{maintenence}$ describes the maintenance factor of PEMFC, and $i_{capital}$ represents the capitalization ratio.

The details for the parameters are given in Table 1.

Fig. 4 shows the multi-objective optimization architecture for the proposed system.

## 4. Objective function for electricity efficiency

Another function that is utilized for the optimization of the hybrid system is to consider the electricity efficiency within 24 h as follows:

$$\eta = \frac{P_G}{P_{wind} + P_{PV}} \tag{40}$$

where, $P_{PV}$ and $P_{wind}$ describe the solar energy absorbed by the PV system and the wind energy absorbed by the wind energy conversion system, respectively and $P_G$ stands for the electrical energy that is generated by the PV, wind energy conversion system, and the PEMFC stack and is obtained as follows:

$$P_G = P_L - P_{shrg} + P_{H_2}^{surplus} + (P_{re} - 0.20 \times P_c) \times 0.88 \tag{41}$$

where, $P_L$ describes the 24-hours demand for total electric energy, $P_{H_2}^{surplus}$ defines the electric energy that is produced by the surplus hydrogen after 24 h's running, $P_{shrg}$ stands for the mismatch between the electric energy and the users' demand, the term $(P_{re} - 0.20 \times P_c) \times 0.88$ determines the remained electricity energy in the battery storage after 24 h system running.

The input wind energy for energy conversion and the input solar energy for the PV conversion are given below:

$$P_{wind} = \int_0^{24} 0.5 \times \rho \times A_{wind} \times \nu^3 dt \tag{42}$$

$$P_{PV} = \int_0^{24} \phi \times A_{PV} \times N_s dt \tag{43}$$

where, $N_s$ stands for the number of PV cells that are put in series and $\rho$ describes the density of the local air.

## 5. Objective function for the energy supply reliability

This section explains the reliability of the energy supply as another part of the cost function for the hybrid system. this term can be determined based on the following equation:

$$\mathbb{R} = \frac{P_L - P_{shrg}}{P_L} \tag{44}$$

**Table 2**
The optimization constraints for the hybrid system.

| Parameter | Initial value | [Min. value, Max. value] | Unit |
|---|---|---|---|
| $P_c$ | 50 | [50, 500] | – |
| $N_s$ | 200 | [50, 200] | – |
| $A_{wind}$ | 50 | [50, 500] | $m^2$ |
| $A_{PEMFC}$ | 1000 | [1000,5000] | $cm^2$ |
| $N_{PEMFC}$ | 100 | [50, 500] | – |

## 6. The total objective function

Based on the definitions in the previous sections, the study aims to optimize three different cost functions including the efficiency of the hybrid system, the capital cost, and the reliability of the energy supply. This makes the problem to be as a multi-objective optimization problem. Here, a developed model of a metaheuristic called Elephant Herding Optimization Algorithm (EHO) is used for this purpose. The optimization is done under some constraints. The total objective function in this study is illustrated below:

$$Maximize(electricity\ efficiency\ (\eta)\ ,\ power\ supply\ reliability\ (\mathbb{R}))$$

$$Minimize\ (Capital\ cost\ (C_T))$$

Subject to:

$$\underline{x}_j \le x_j \le \bar{x}_j$$

where, $\underline{x}_j$ and $\bar{x}_j$ stand for the lower and the upper limitations of the $j$th constraint. Five main parameters for the optimization of the above problem are given below (see Table 2).

## 7. Balanced elephant herding optimization algorithm

Evolutionary and metaheuristic algorithms (metaheuristics) are very powerful tools of artificial intelligence to solve optimization problems through intelligent methods and are nowadays widely used in several branches of science and engineering. These algorithms, which generally simulate the natural processes, are search methods that search for the best possible solution in the possible search space for an optimization problem. An important case that should be considered in metaheuristics is the dynamic balance between diversification and intensification. Diversification performs an extended searching in the search space and intensification indicates the solutions experienced during searching in the solution space. Considering the correct trade-off between these two strategies gives better solution space to the algorithms and decreases time-wasting. There are several models of metaheuristics such as Variance Reduction of Gaussian Distribution (VRGD) (Namadchian et al., 2016), Butterfly Optimization Algorithm (BOA) (Arora and Singh, 2019), Owl Search Algorithm (OSA) (Jain et al., 2018), Emperor Penguin Optimizer (EPO) (Dhiman and Kumar, 2018), Improved Cat Swarm Optimization (ICSO) algorithm (Kumar and Singh, 2018), World Cup Optimization (WCO) algorithm (Razmjooy et al., 2016), sunflower optimization (SFO) algorithm (Gomes et al., 2019), and Elephant herding optimization (EHO) (Wang et al., 2016).

Wang et al. proposed a new bio-inspired algorithm based on elephant herding behavior (Wang et al., 2016). Elephants are a kind of mammal animals that have big sizes. These animals have a long trunk that helps to breathe, lifting objects and drinking water. They also have strong legs to carry their weights. Naturally, in contrast, the male elephants that like to live alone upon growing up, female elephants have social behaviors and like to comprise the clans of females and the calves. They live in several clusters under the leadership of a matriarch that is usually the oldest one. However male elephants live independently from their family

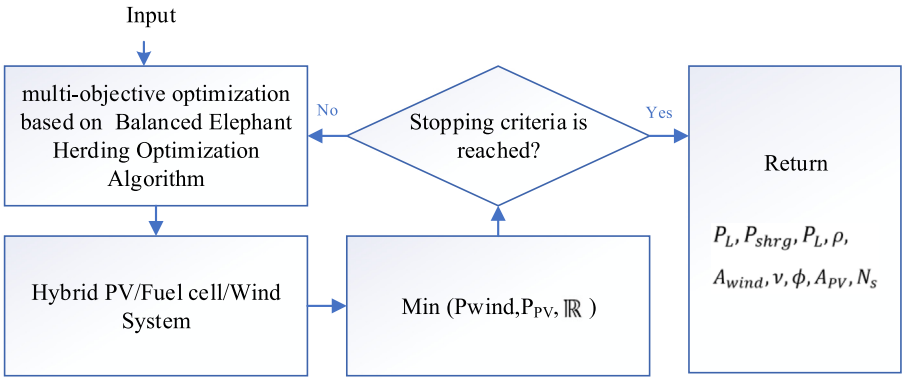


**Fig. 4.** The multi-objective optimization architecture for the proposed system.

group, they can connect with the family members over low-frequency vibrations. Each member of the elephant clans has high attention to the calves as the of a family group. This specific behavior has been a reason for proposing a new bio-inspired that is called Elephant Herding Optimization (EHO) Algorithm. The EHO Algorithm is based on the following characteristics:

### 7.1. Clan operator

As before mentioned, each clan has been led under the leadership of a matriarch. This case causes that matriarch *ci* affecting the next position of the elephants in clan *ci*. Therefore, the new position for the elephant *j* in clan *ci* ($x_{ci,j}^{new}$) is achieved as follows:

$$x_{ci,j}^{new} = x_{ci,j} + \alpha \times \left(x_{ci}^{best} - x_{ci,j}\right) \times r \tag{45}$$

where, $x_{ci,j}$ stands for the old position of elephant *j* in clan *ci*, $x_{ci}^{best}$ describes matriarch *ci* that has the best solution in clan *ci*, $\alpha$ represents a scale factor to determine the impact of matriarch *ci* on $x_{ci,j}$ In the range [0, 1] and $r \in [0, 1]$ is another random value.

And the updating formulation for the fittest elephant in each clan is achieved as follows:

$$x_{ci,j}^{new} = \beta \times x_{ci}^{center} \tag{46}$$

where $\beta$ stands for a factor to define the effect of the $x_{ci}^{center}$ on $x_{ci,j}^{new}$ in the range [0, 1].

In the above equation, $x_{ci,j}^{new}$ is obtained by considering the information from the elephants in clan *ci* and $x_{ci}^{center}$ determines the center of clan *ci*. For the *d*th dimension, this term can be evaluated through *D* evaluations as follows:

$$x_{ci}^{center} = \frac{1}{n_{ci}} \sum_{j=1}^{n_{ci}} x_{ci,j}^{d} \tag{47}$$

where *d* determines the *d*th dimension in the range [1, D], *D* stands for the total dimension, $n_{ci}$ describes the total number of elephants in the clan *ci*, and $x_{ci,j}^{d}$ describes the *d*th case of the elephant candidate $x_{ci,j}$.

### 7.2. Separating operator

As before mentioned, male elephants live independently from the family when they have grown up. This feature is modeled in the EHO algorithm as a separating operator. This feature is modeled as follows:

$$x_{ci}^{worst} = \underline{x} + \left(1 + \bar{x} - \underline{x}\right) \times \delta \tag{48}$$

where, $x_{ci}^{worst}$ describes the worst elephant individual in clan *ci*, $\delta \in [0, 1]$ is a random uniform distribution value, and $\underline{x}$ and $\bar{x}$ represent the minimum and the maximum limitations of the elephant individual position, respectively.

More information about the EHO algorithm can be studied (Wang et al., 2016).

### 7.3. The balanced EHO algorithm

However, the EHO algorithm is a new and high-performance algorithm for optimization, it has also some issues that should be resolved. The main problem is the early convergence of the EHO algorithm. In this algorithm, the individuals gradually move in the search space near the best general optimum point and do not explore the rest of the space which is due to the inadequate balance mechanism between local and global search. This study proposes an improved version of the EHO algorithm for resolving this problem.

Here, the Lévy flight mechanism has been adopted for developing the EHO algorithm. This mechanism has a high capability to resolve premature convergence of the algorithm (Cao et al., 2019a,b; Fei et al., 2019) as a prominent shortcoming of the EHO. Lévy flight (LF) simulates a random walk mechanism for viable handling of the local search (Choi and Lee, 1998). This Lévy flight mechanism is modeled as follows:

$$Le(w) \approx w^{-1-\tau} \tag{49}$$

$$w = A \times |B|^{-1/\tau} \tag{50}$$

$$\sigma^2 = \left\{ \frac{\Gamma(1+\tau)}{\tau\,\Gamma((1+\tau)/2)} \frac{\sin(\pi\tau/2)}{2^{(1+\tau)/2}} \right\}^{\frac{2}{\tau}} \tag{51}$$

where, $\Gamma(.)$ is Gamma function, $0 < \tau \leq 2$, $A \sim N(0, \sigma^2)$, $B \sim N(0, \sigma^2)$, *w* stands for the step size, $\tau$ describes Lévy index, and $A/B \sim N(0, \sigma^2)$ point to the samples formed by a Gaussian distribution with a mean value of zero and variance of $\sigma^2$. In this study, $\tau = 3/2$ (Li et al., 2018).

Based on the defined mechanism, the new updated equation for the clan and the separating operators are as follows:

$$x_{ci,j}^{new} = x_{ci,j} + \alpha \times \left(x_{ci}^{best} - x_{ci,j}\right) \times r \times \mathrm{Le}(\delta) \tag{52}$$

$$x_{ci}^{worst} = \underline{x} + \left(1 + \bar{x} - \underline{x}\right) \times \delta \times \mathrm{Le}(\delta) \tag{53}$$

where, $x_{ci,j}^{new}$ is the newly updated position for the elephant *j* in clan *ci* ($x_{ci,j}^{new}$), and $x_{ci}^{worst}$ describes the new updated worst elephant individual in clan *ci*.

Besides, to guarantee of achieving the best solution candidates, fitter candidates have been kept:

$$x_{ci,j}^{new} = \begin{cases} x_{ci,j}^{new} & F\left(x_{ci,j}^{new}\right) > F(x_{ci,j}^{new}) \\ x_{ci,j}^{new} & otherwise \end{cases} \tag{54}$$

$$x_{ci}^{worst} = \begin{cases} x_{ci}^{worst} & F\left(x_{ci}^{worst}\right) > F(x_{ci}^{worst}) \\ x_{ci}^{worst} & otherwise \end{cases} \tag{55}$$

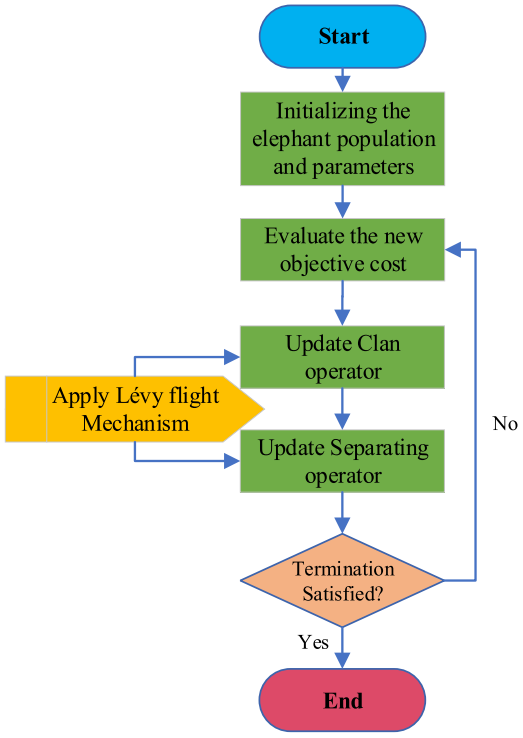


**Fig. 5.** The block diagram of the proposed BEHO.

Fig. 5 shows the block diagram of the presented BEHO.

## 8. Algorithm validation

In this section, to indicate the ability of the presented BEHO algorithm, it is validated by implementing it into some different functions. The results also compared with some different state of the art algorithms like genetic algorithm (GA) (Holland, 1992), particle swarm optimization algorithm (PSO) (Bansal, 2019), fluid search optimization algorithm (FSO) (Dong and Wang, 2018), world cup optimization algorithm (WCO) (Razmjooy et al., 2016), and the basic Elephant Herd Optimization (EHO) algorithm (Wang et al., 2016). The configuration of the selected laptop for simulation is Intel® Core™ i7-4720 HQ CPU@2.60 GHz with 16 GB RAM and the platform for the simulation is MATLAB R2017b. Table 3 indicates the utilized equations and their constraints for the validation with 30 dimensions.

After applying the utilized algorithms to the functions, the results for validation are achieved and provided in Table 4. This Table indicates the standard deviation value and the mean value of the compared methods by assuming 30-dimensions.

As can be seen, the best results are achieved by the EHO family for the adopted benchmark functions. The simulation for each algorithm has been run for 30 times to show its precision and standard deviation value. due to the minimum value of the BEHO algorithm, it can be considered as the highest accuracy algorithm among the compared methods. Besides, due to the low value of the standard deviation value, it has shown the highest precision among the others.

## 9. Simulation results

As before mentioned, the main purpose is to optimize a three-term multi-objective optimization including the energy supply reliability, the electricity efficiency, and the capital cost based on a newly introduced metaheuristic to achieve the best solution

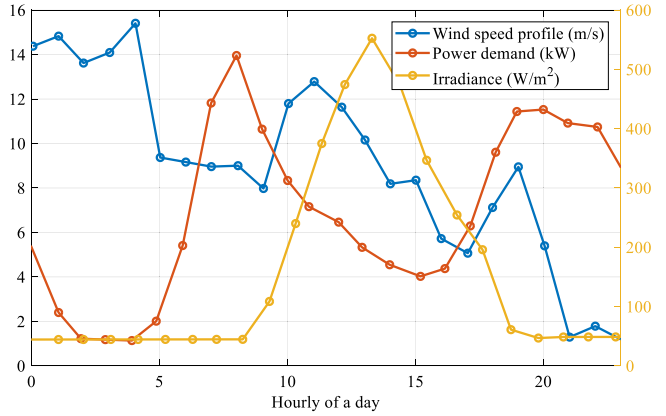


**Fig. 6.** Hourly profile of wind speed data, solar irradiance data, and the power demand data.

on a hybrid PV/wind/PEMFC/battery system. Fig. 6 Indicate the hourly profile of the solar irradiance data, wind speed data, and the power demand data, respectively that are used as the inputs for the case study. As can be seen, the wind speed during the 24 h starts with about 14.2 m/s in 12:00 and then after some descending oscillations, it reaches its lowest value about 1.1 m/s in 24:00. The results also show that from 8:00 to 13:00, an increasing irradiation occurs. In contrast, from 13:00 to about 18:00, the irradiance behaves as a downtrend process and after 18:00, this minimum value continues in about a side way value. Finally, by considering the power demand, it is clear the power demand in 12:00 is about 5.2 kW and this changes until 8:00 with maximum power demand. Another time of high power demand in the range 17:00 to 24.

For more clarifications about the Pareto solution set, the cost values of 300 optimal designs have been normalized in the range [0,1] and the results are shown in Table 5 and Fig. 7. From the results, it is clear that there are three scenarios for the system analysis: the minimum capital cost (S1), the maximum energy supply reliability (S2), and the maximum electricity efficiency (S3). Here, the S1 shows the high energy efficiency from 14.68% to 15.82%, with the corresponding cost from 2461$/year to 3083 $/year with energy supply reliability from 77.20% to 80.47%. The S3 shows the low capital cost from 2834 $/year to 2934 $/year and the electricity efficiency in the range 17.53% and 18.74% along with energy supply reliability from 76.24% to 76.89%. Finally, S2 gives a high energy supply reliability in the range 85.36% and 87.82% with the capital cost from 2846 $/year to 3373 $/year and with the electricity efficiency in the range 8.61% and 11.75%.

Therefore, if the main objective is to focus on the lower capital cost of the hybrid system, *S*1 (with scarifying the energy supply reliability), is the best selection, if the main objective is to emphasize on the higher energy supply reliability, *S*2 gives the best selection (of course by losing the ability for the other two aspects, and if the main objective is to obtain higher electricity efficiency of the hybrid system with losing the other two aspects, *S*3 is the best selection.

For more clarification of the results, the study uses the approximated Pareto front. Generally, to obtain the desired performance, the decision variables values can be found by the decision makers. In other words, these results help the decision variables to consider what should be sacrificed to obtain better efficiency for the other objective function. Besides, after determining the design variables, the dynamic response of the units can be observed by the provided models according to the weather and load conditions. By this way, the design makers can recognize how to choose the size of units in the hybrid system for decreasing the

**Table 3**
The utilized benchmarks for efficiency analysis.

| Function | Equation | Constraint |
|---|---|---|
| Ackley | $f_1(x) = -20exp\left(-0.2\sqrt{\frac{1}{D}\sum_{i=1}^{D}x_i^2}\right) - exp\left(\frac{1}{D}\sum_{i=1}^{D}cos(2\pi x_i)\right) + 20 + e$ | $[-10, 10]$ |
| Rastrigin | $f_2(x) = 10D + \sum_{i=1}^{D}\left(x_i^2 - 10\cos(2\pi x_i)\right)$ | $[-512, 512]$ |
| Rosenbrock | $f_3(x) = \sum_{i=1}^{D-1}\left(100\left(x_i^2 - x_{i+1}\right) + (x_i - 1)^2\right)$ | $[-2.045, 2.045]$ |
| Sphere | $f_4(x) = \sum_{i=1}^{D}x_i^2$ | $[-512, 512]$ |

**Table 4**
The validation results of the compared methods.

| Benchmark | | BEHO | EHO (Wang et al., 2016) | GA (Holland, 1992) | PSO (Bansal, 2019) | WCO (Razmjooy et al., 2016) | FSO (Dong and Wang, 2018) |
|---|---|---|---|---|---|---|---|
| $f_1$ | mean | 0.00 | 9.38e−18 | 4.18e−2 | 7.85 | 4.28e−3 | 5.34e−16 |
| | std | 0.00 | 0.00 | 3.53e−2 | 2.16 | 2.14e−3 | 0.00 |
| $f_2$ | mean | 0.00 | 1.98 | 70.61 | 74.24 | 2.19 | 3.42 |
| | std | 0.00 | 1.58 | 1.66 | 8.96 | 4.35 | 3.27 |
| $f_3$ | mean | 5.48 | 5.84 | 35.41 | 200.1 | 13.16 | 8.64 |
| | std | 3.61 | 1.32 | 27.15 | 59.00 | 4.62 | 2.56 |
| $f_4$ | mean | 0.00 | 5.28e−14 | 1.62e−4 | 7.59e−4 | 5.27e−9 | 2.16e−12 |
| | std | 0.00 | 2.37e−18 | 2.57e−5 | 4.93e−4 | 2.74e−9 | 4.93e−17 |

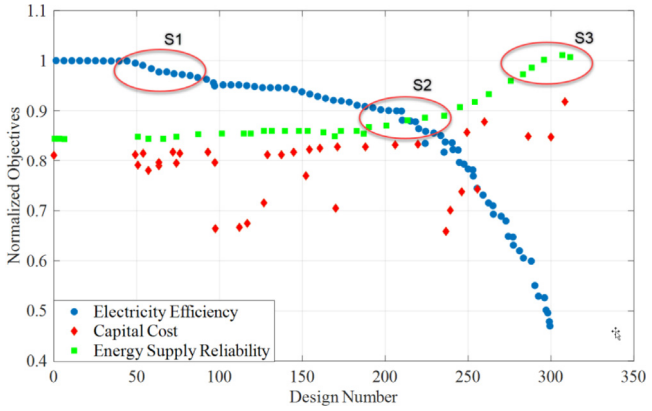


**Fig. 7.** Normalized objectives for 300 designs of the proposed hybrid system..

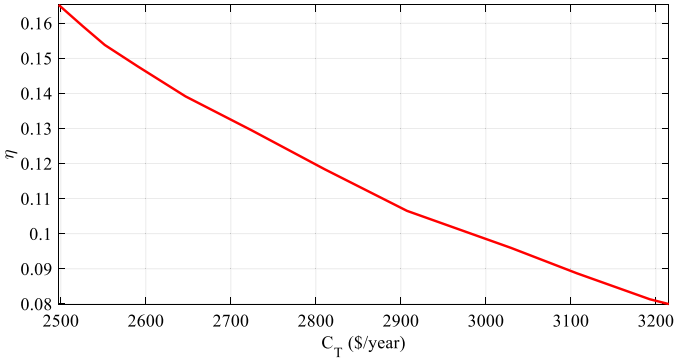


**Fig. 8.** Pareto front of the electricity efficiency and the energy supply reliability.

renewable energy fluctuation by the help of Pareto front (see Fig. 8).

Therefore, based on the above results and the Pareto front, the decision-makers can provide the best selection based on their positions.

**Table 5**
The cost function values for different scenarios.

| Cost function | S1 | S2 | S3 |
|---|---|---|---|
| $\eta$ (%) | 14.68–15.82 | 8.61–11.75 | 17.53–18.74 |
| $\mathbb{R}$ (%) | 77.20–80.47 | 85.36–87.82 | 76.24–76.89 |
| $C_T$ ($/year) | 2461–3083 | 2846–3373 | 2834–2934 |

## 10. Conclusions

This study proposed a multi-objective optimization structure for a hybrid PV/Wind/PEMFC/Battery system. The optimization configuration included three parts of cost minimization, energy supply reliability maximization, and electricity efficiency maximization. The optimization process was performed using a new balanced model of the Elephant Herding Optimization (BEHO) Algorithm. The purpose of the study was to determine the Pareto surface of the problem to make the decision operation easy for decision-makers.

The proposed method analyzed three different scenarios including minimum capital cost (S1), maximum energy supply reliability (S2), and maximum electricity efficiency (S3). The final results showed that the only case for selecting the best configuration is to check the Pareto solution set. In addition to the parameters that are considered for the optimization in this work, there are some other parameters that can effect on the system, for example, PEMFC area and number of PEMFC cells that give an inspiration to work on them in the future work.

## CRediT authorship contribution statement

**Yan Cao:** Conceptualization, Data curation, Writing - original draft, Writing - review & editing. **Hui Yao:** Conceptualization, Data curation, Writing - original draft, Writing - review & editing. **Zhijie Wang:** Conceptualization, Data curation, Writing - original draft, Writing - review & editing. **Kittisak Jermsittiparsert:** Conceptualization, Data curation, Writing - original draft, Writing - review & editing. **Nasser Yousefi:** Conceptualization, Data curation, Writing - original draft, Writing - review & editing.

## Declaration of competing interest

The authors declare that they have no known competing financial interests or personal relationships that could have appeared to influence the work reported in this paper.

## Acknowledgments

This paper is supported by Shaanxi Innovation Capability Support Plan, China (Grant: 2018TD-036), Shaanxi Natural Science Basic Research, China Project (Grant: S2019-JC-YB-2897), and Research Project of Graduate Education and Teaching Reform of Xi'an Technological University in 2017.

## References

Aghajani, Gholamreza, Ghadimi, Noradin, 2018. Multi-objective energy management in a micro-grid. Energy Rep. 4, 218–225.
Akbary, Paria, et al., 2019. Extracting appropriate nodal marginal prices for all types of committed reserve. Comput. Econ. 53 (1), 1–26.
Arora, S., Singh, S., 2019. Butterfly optimization algorithm: a novel approach for global optimization. Soft Comput. 23 (3), 715–734.
Bagal, Hamid Asadi, et al., 2018. Risk-assessment of photovoltaic-wind-battery-grid based large industrial consumer using information gap decision theory. Sol. Energy 169, 343–352.
Bansal, J.C., 2019. Particle swarm Optimization. In: Evolutionary and Swarm Intelligence Algorithms. Springer, pp. 11–23.
Cao, Y., Li, Y., Zhang, G., Jermsittiparsert, K., Razmjooy, N., 2019a. Experimental modeling of PEM fuel cells using a new improved seagull optimization algorithm. Energy Rep. 5, 1616–1625.
Cao, Y., Wu, Y., Fu, L., Jermsittiparsert, K., Razmjooy, N., 2019b. Multi-objective optimization of a PEMFC based CCHP system by meta-heuristics. Energy Rep. 5, 1551–1559.
Chedid, R., Akiki, H., Rahman, S., 1998. A decision support technique for the design of hybrid solar-wind power systems. IEEE Trans. Energy Convers. 13 (1), 76–83.
Chen, H., Yang, C., Deng, K., Zhou, N., Wu, H., 2017. Multi-objective optimization of the hybrid wind/solar/fuel cell distributed generation system using Hammersley Sequence Sampling. Int. J. Hydrogen Energy 42 (12), 7836–7846.
Choi, C., Lee, J.-J., 1998. Chaotic local search algorithm. Artif. Life Robot. 2 (1), 41–47.
Dhiman, G., Kumar, V., 2018. Emperor penguin optimizer: A bio-inspired algorithm for engineering problems. Knowl.-Based Syst. 159, 20–50.
Dong, R., Wang, S., 2018. New optimization algorithm inspired by fluid mechanics for combined economic and emission dispatch problem. Turk. J. Electr. Eng. Comput. Sci. 26 (6), 3305–3318.
Ebrahimian, Homayoun, et al., 2018. The price prediction for the energy market based on a new method. Econ. Res.-Ekon. Istraž. 31 (1), 313–337.
Eslami, Mahdiyeh, et al., 2019. A new formulation to reduce the number of variables and constraints to expedite SCUC in bulky power systems. Proc. Natl. Acad. Sci. India A 89 (2), 311–321.
Fathi, G., Ghadimi, N., Akbarimajd, A., Dehkordi, A.B., 2020. Stochastic-based energy management of DC microgrids. In: Risk-Based Energy Management. Elsevier, pp. 31–47.
Fei, X., Xuejun, R., Razmjooy, N., 2019. Optimal configuration and energy management for combined solar chimney, solid oxide electrolysis, and fuel cell: a case study in Iran. Energy Sources A 1–21.
Firouz, Mansour Hosseini, Ghadimi, Noradin, 2016. Concordant controllers based on FACTS and FPSS for solving wide-area in multi-machine power system. J. Intell. Fuzzy Systems 30 (2), 845–859.
Gheydi, Milad, Nouri, Alireza, Ghadimi, Noradin, 2016. Planning in microgrids with conservation of voltage reduction. IEEE Syst. J. 12 (3), 2782–2790.
Gollou, Abbas Rahimi, Ghadimi, Noradin, 2017. A new feature selection and hybrid forecast engine for day-ahead price forecasting of electricity markets. J. Intell. Fuzzy Systems 32 (6), 4031–4045.
Gomes, G.F., da Cunha, S.S., Ancelotti, A.C., 2019. A sunflower optimization (SFO) algorithm applied to damage identification on laminated composite plates. Eng. Comput. 35 (2), 619–626.
Guo, K., Prévoteau, A., Rabaey, K., 2017. A novel tubular microbial electrolysis cell for high rate hydrogen production. J. Power Sources 356, 484–490.
Hamian, Melika, et al., 2018. A framework to expedite joint energy-reserve payment cost minimization using a custom-designed method based on Mixed Integer Genetic Algorithm. Eng. Appl. Artif. Intell. 72, 203–212.
Holland, J.H., 1992. Genetic algorithms. Sci. Am. 267 (1), 66–73.
Hoogers, G., 2002. Fuel Cell Technology Handbook. CRC press.
Hosseini Firouz, Mansour, Ghadimi, Noradin, 2016. Optimal preventive maintenance policy for electric power distribution systems based on the fuzzy AHP methods. Complexity 21 (6), 70–88.
Jain, M., Maurya, S., Rani, A., Singh, V., 2018. Owl search algorithm: a novel nature-inspired heuristic paradigm for global optimization. J. Intell. Fuzzy Systems 34 (3), 1573–1582.
Khodaei, Hossein, et al., 2018. Fuzzy-based heat and power hub models for cost-emission operation of an industrial consumer using compromise programming. Appl. Therm. Eng. 137, 395–405.
Kiran, P., Chandrakala, K.V., 2020. Variant Roth-Erev reinforcement learning algorithm-based smart generator bidding as agents in electricity market. In: Soft Computing for Problem Solving. Springer, pp. 981–989.
Kumar, Y., Singh, P.K., 2018. Improved cat swarm optimization algorithm for solving global optimization problems and its application to clustering. Appl. Intell. 48 (9), 2681–2697.
Leng, Hua, et al., 2018. A new wind power prediction method based on ridgelet transforms, hybrid feature selection and closed-loop forecasting. Adv. Eng. Inf. 36, 20–30.
Li, X., Niu, P., Liu, J., 2018. Combustion optimization of a boiler based on the chaos and levy flight vortex search algorithm. Appl. Math. Model. 58, 3–18.
Liu, J., Chen, C., Liu, Z., Jermsittiparsert, K., Ghadimi, N., 2020. An IGDT-based risk-involved optimal bidding strategy for hydrogen storage-based intelligent parking lot of electric vehicles. J. Energy Storage 27, 101057.
Liu, Yang, Wang, Wei, Ghadimi, Noradin, 2017. Electricity load forecasting by an improved forecast engine for building level consumers. Energy 139, 18–30.
Mirzapour, Farzaneh, et al., 2019. A new prediction model of battery and wind-solar output in hybrid power system. J. Ambient Intell. Humaniz. Comput. 10 (1), 77–87.
Namadchian, A., Ramezani, M., Razmjooy, N., 2016. A new Meta-Heuristic algorithm for optimization based on variance reduction of Guassian distribution. Majlesi J. Electr. Eng. 10 (4), 49.
Razmjooy, N., Khalilpour, M., Ramezani, M., 2016. A new Meta-Heuristic Optimization algorithm inspired by FIFA world cup competitions: Theory and its application in PID designing for AVR system. J. Control Autom. Elect. Syst. 27 (4), 419–440.
Restrepo, C., Konjedic, T., Garces, A., Calvente, J., Giral, R., 2014. Identification of a proton-exchange membrane fuel cell's model parameters by means of an evolution strategy. IEEE Trans. Ind. Inf. 11 (2), 548–559.
Saeedi, Mohammadhossein, et al., 2019. Robust optimization based optimal chiller loading under cooling demand uncertainty. Appl. Therm. Eng. 148, 1081–1091.
Tan, L., Yang, C., Zhou, N., 2015. Synthesis/design optimization of SOFC–PEM hybrid system under uncertainty. Chin. J. Chem. Eng. 23 (1), 128–137.
Wang, G.-G., Deb, S., Gao, X.-Z., Coelho, L.D.S., 2016. A new metaheuristic optimisation algorithm motivated by elephant herding behaviour. Int. J. Bio-Inspir. Comput. 8 (6), 394–409.
Yang, C., Zhang, Y.-y., Xu, Z.-y., 2007. Numerical simulation of heat and mass transfer in Sofc. J. Syst. Simul. 14.